IEEE Open Journal of Vehicular Technology

Received 2 March 2022; accepted 24 March 2022. Date of publication 4 April 2022;
date of current version 3 May 2022. The review of this article was coordinated by Editor Ping Wang.

Digital Object Identifier 10.1109/OJVT.2022.3164461

Software-Defined Radio-Based Evaluation Platform for Highly Mobile IEEE 802.22 System

RUITING OUYANG [1] (Member, IEEE), TAKESHI MATSUMURA [1,2] (Member, IEEE), KEIICHI MIZUTANI [1,3] (Member, IEEE), AND HIROSHI HARADA [1] (Member, IEEE)

[1]Graduate School of Informatics, Kyoto University, Kyoto 606-8501, Japan
[2]Wireless Systems Laboratory, National Institute of Information and Communications Technology, Yokosuka 239-0847, Japan
[3]School of Platforms, Kyoto University, Kyoto 606-8501, Japan

CORRESPONDING AUTHOR: RUITING OUYANG (e-mail: ouyang@dco.cce.i.kyoto-u.ac.jp)

This paper was presented in part at WPMC2020, Virtual Events in Part, Oct. 2020, DOI: 10.1109/WPMC50192.2020.9309487. This work was supported in part by the Ministry of Internal Affairs and Communications in Japan under Grant JPJ000254, and in part by the Ministry of Internal Affairs and Communications in Japan under Grant SCOPE JPJ000595.

ABSTRACT Wide-area communication systems using TV white space (TVWS) are promising technologies capable of full-coverage and cost-effective vehicular and transportation communications owing to their excellent propagation characteristics. IEEE 802.22 was developed as a TVWS-based fixed communication standard to support a wide coverage area of 10–30 km. To cope with the various applications in mobile communication, the transmission performance needs to be enhanced and evaluated. Thus, it becomes necessary to develop an experimental platform to enable the flexible implementation of transmitter and receiver algorithms. In this regard, we propose a software-defined radio (SDR)-based evaluation platform enabling the bench testing of physical layer (PHY) performance for highly mobile IEEE 802.22 communication systems. Using this platform, radio frequency signals can be transmitted and received using reconfigurable hardware and software, with the received baseband signals being recorded and stored by the SDR device. The stored data were post-processed using a MATLAB-based program to evaluate the transmission performance. The performance achieved by SDR-based evaluation system is similar to computer simulations, thereby demonstrating the feasibility of highly mobile IEEE 802.22 communication systems. Moreover, the proposed evaluation platform is available for future field experiments to encourage the development and evaluation of novel PHY algorithms.

INDEX TERMS IEEE 802.22, prototype, software-defined radio, vehicular network, wireless regional area network.

I. INTRODUCTION

In the current Internet-of-Things (IoT) era, various smart devices are being connected to the Internet. For instance, with the advances in intelligence, vehicular networks with full-range wireless connections between vehicles and the surrounding infrastructure serve as the most promising technology that enables the management of traveling vehicles and mitigates social traffic problems in an environment-friendly manner [2]. In current vehicular networks, several wireless communication systems such as the IEEE 802.11p [3], ARIB STD-T109 [4], and LTE-based systems [5] have already been installed, and also the potential for cutting-edge applications will be demonstrated with 5G new radio (NR)-based communication systems in near-future vehicular networks [6].

The IEEE 802.11p-based dedicated short-range communication system is a wireless technology for vehicular communication designed to support safety applications via vehicle-to-vehicle (V2V) and vehicle-to-infrastructure (V2I) communications [3]. Because of the limited communication coverage of the IEEE 802.11p system, multi-hop communication is necessary to achieve long-range multicasting for a full-range vehicular network. To support multi-hop communication, onboard units (OBUs) and roadside units (RSUs) in conformity with the IEEE 802.11p standard need to be installed

in vehicles and infrastructure, respectively, to enable interconnection [7]. The LTE-based vehicle-to-everything (V2X) standard was released by 3GPP within its Release 14 guidelines, also known as LTE-V2X [5]. With the evolution of cellular-based V2X systems, the 5G NR-based V2X standard was released within Release 16 and known as NR-V2X [6]. However, the coverage of LTE-V2X and NR-V2X systems is limited to approximately 300 m in a non-line-of-sight environment with relatively low latency requirements [8]. To achieve a full-range vehicular network in rural areas, many RSUs are necessary for IEEE 802.11p, LTE-V2X, and NR-V2X networks; however, they lead to frequent handovers from one RSU to the next owing to the limited coverage and high vehicle velocities. The ARIB STD-T109 standard was further developed based on IEEE 802.11p in Japan, and it is operated at 760 MHz with an allocated bandwidth of 10 MHz. The ARIB STD-T109 has a relatively wide supporting range of up to 900 m, while the bandwidth is insufficient to support annually increasing capacity demands. Consequently, a wideband vehicular communication system is required to cover wide areas, particularly in rural districts.

Nowadays, since the availability of radio spectrum is drying up, the utilization of VHF and UHF bands below 700 MHz is expected as a viable solution to spectrum scarcity. Although the frequency bands are currently used by TV broadcasting operators as primary users, other users and operators of fixed and/or mobile communications—that is, secondary users—use the bands via dynamic spectrum-sharing technologies [9] in which primary and secondary users register their technical specifications in a spectrum database, which then calculates the protection area of primary users based on the registered information and notifies secondary users of available spectrum. These bands are known as TV white spaces (TVWSs).

TVWSs have the potential to provide wide-coverage, large-capacity, and cost-effective connectivity for vehicular networks owing to their superior propagation properties and high spectrum availability, which could lead to advanced heterogeneous vehicular networks [9]–[11]. The IEEE 802.22 network was the world's first standardized communication system for a fixed point-to-multipoint wireless regional area network (WRAN) system in TVWSs [12]. Moreover, the IEEE 802.22-based WRAN is capable of a wide communication range of 10–30 km, allowing up to 512 customer premise equipment (CPE) devices to access the same base station (BS) using orthogonal frequency division multiple access (OFDMA) techniques. Therefore, the application of the IEEE 802.22 system to mobile communication is one of the most cost-effective measures for offering long-distance and large-scale vehicular networks. If the IEEE 802.22-based WRAN is adapted for highly mobile communication scenarios, vehicles sparsely and widely distributed in rural areas could get the ability to connect to the network directly and individually without RSUs. Consequently, the physical number of RSUs could be reduced as well as the overhead caused by frequent handovers, leading to more efficient communication systems in terms of deployment cost and performance. However, the IEEE 802.22 system was standardized as a fixed communication system, and the highly mobile and long-delay multipath fading propagation environment degrades its transmission performance. Thus, it is necessary to develop robust physical layer (PHY) receiving schemes to enhance its mobility, particularly in a long-delay multipath fading environment.

Recently, several studies have investigated reliable receiving schemes and performance evaluation for IEEE 802.22-based highly mobile communication systems [13], [14]. These studies have focused on PHY performance evaluations based on computer simulations. In addition, several studies have reported their experimental evaluations of IEEE 802.22 prototypes [15], [16], focusing on the evaluation of conventional IEEE 802.22 systems with fixed CPE devices. However, there are no prototypes or devices that include receiving schemes to realize highly mobile communication systems.

For algorithm debugging and evaluation during the development of receiving schemes in highly mobile environments, an experimental platform that enables simple and flexible implementation of various receiving schemes is crucial. Moreover, from the radio propagation point of view, some signal deterioration factors such as imperfect frequency filtering, the phase noise of oscillators, and the nonlinearity of amplifiers are barely considered. Therefore, an experimental measurement and evaluation platform is required for the receiver design of a near-future IEEE 802.22-based highly mobile communication system. To the best of our knowledge, no appropriate experimental evaluation platform is available for the flexible design of such systems.

In this study, a software-defined radio (SDR)-based experimental platform is developed for the experimental measurement and evaluation of the receiving scheme of the IEEE 802.22 PHY. The developed platform comprises an IEEE 802.22 radio frequency (RF) signal transmitter, IEEE 802.22 RF signal receiver, and digital baseband signal processor. As the RF signal transmitter, a signal generator (SG) or a compact IEEE 802.22-based prototype is applied to generate the IEEE 802.22 signal in conformity with the standardized frame structure, and an SDR-based device is used as the IEEE 802.22 RF signal receiver. The SDR-based receiver allows offline processing of digital baseband signals and performance evaluation even using a low-end laptop. The developed evaluation platform is available for both laboratory and field experiments, enabling easy receiving algorithm evaluation and validation during the development of IEEE 802.22-based highly mobile communication systems. To validate the developed experimental platform and evaluate existing receiving schemes for IEEE 802.22-based highly mobile communication systems, a laboratory experiment is conducted.

The main contributions of this study are summarized as follows:

- The developed framework includes the IEEE 802.22 transmitter utilizing an SG or compact prototype. The SG-based transmitter is fully software-controlled, and the prototype-based transmitter can be implemented using programmable hardware.

TABLE 1 System Parameters of IEEE 802.22 [12]

Item	Specification
Frequency range	54 – 862 MHz
Channel bandwidth	6, 7, or 8 MHz
Data rate	4.54 – 22.69 Mbit/s
Transmit equivalent isotropic radiated power (EIRP)	4 W maximum
Multiple access	OFDMA
Duplex	Time division duplex (TDD)
FFT size	2,048
CP length	1/4, 1/8, 1/16, 1/32

- The developed framework includes an SDR-based RF signal receiver and offline digital baseband signal processor that allows simple signal processing, even on a low-end laptop.
- In the digital signal processor of the experimental platform, a timing synchronization scheme is proposed and implemented to synchronize the received IEEE 802.22 signal—even in a highly mobile environment—and an estimation and compensation scheme for the carrier frequency offset (CFO) between the BS and the CPE is also implemented.
- Laboratory experiments were conducted on the IEEE 802.22-based system to measure the bit error rates (BERs) in a harsh multipath fading environment with a relatively high Doppler frequency by using the developed platform and a fading emulator (FE). As a result, a required BER of 2×10^{-4} was achieved, even in a highly mobile environment.

The remainder of this paper is organized as follows. In Section II, the general specifications of the IEEE 802.22 standard and the highly mobile IEEE 802.22 system are described. In Section III, the proposed evaluation platform and its corresponding configuration are explained. The experimental laboratory results are described in Section IV. Finally, Section V concludes the paper.

II. IEEE 802.22 SYSTEM

A. OVERVIEW

IEEE 802.22 [12] was standardized as the first fixed point-to-multipoint WRAN system to support unlicensed operations in the TV broadcast band using cognitive radio technologies. Table 1 lists the PHY configuration parameters for the IEEE 802.22 system. The PHY parameters are designed to enable a transmission range of up to 30 km, where the coverage can be expanded to 100 km with appropriate scheduling at the BS. To support such wide coverage, the minimum receiver sensitivity required to achieve a BER of less than 2×10^{-4} at the BS and CPE are –94.5 dBm and –91.3 dBm, respectively, for quadrature phase shift keying (QPSK) with a code rate of 1/2 in the case of a 6 MHz channel bandwidth.

In the normal mode, one superframe includes 16 frames with a frame length of 10 ms. The first frame in each superframe includes a superframe preamble, frame preamble, superframe control header (SCH), frame control header (FCH), and data payload. For the remaining 15 frames, the frame preamble, frame header, and data payload are included.

The superframe preamble used for signal detection and coarse frequency synchronization has a duration of one OFDM symbol consisting of a cyclic prefix (CP) of 1/4 of the OFDM symbol duration and four repetitions of a short training sequence (STS) in the time domain. Here, the CP is the same as that of the STS. The frame preamble used for fine frequency synchronization and channel estimation has a CP of 1/4 of the OFDM symbol duration and two repetitions of the long training sequence (LTS) in the time domain. Similarly, the CP is the second half of the LTS.

Each frame comprises 26–41 OFDM symbols based on the CP length and channel bandwidth. One frame is divided into downstream (DS) and upstream (US) subframes. A transmit/receive transition gap is allocated between the DS and US subframes to secure the transition time from DS to US at the CPE.

B. HIGHLY MOBILE IEEE 802.22 SYSTEM

Owing to the excellent propagation properties and large CPE capacity of each BS, the application of IEEE 802.22 to a highly mobile communication system is one of the most promising approaches to cope with vehicular communication in rural areas, where vehicles are sparsely distributed and move at a high velocity [13], [14].

However, IEEE 802.22 was originally standardized as a fixed communication system, and the propagation channel was considered invariant in the time domain or with a relatively small Doppler shift. By contrast, the high velocity of CPEs induces a considerable Doppler shift, which increases the complexity of the receiver design—including frame detection, frequency synchronization, and channel estimation. To improve system performance and meet communication requirements, several technologies have been developed for highly mobile IEEE 802.22 communication systems. In [13] and [14], a novel channel estimation scheme and frequency synchronization scheme adhering to the PHY design in the IEEE 802.22 standard have been proposed to enhance mobility. With ideal timing synchronization, the feasibility of the novel channel estimation and frequency synchronization schemes were confirmed using computer simulation in a harsh propagation environment with vehicle velocities of up to 80 km/h.

III. PROPOSED EXPERIMENTAL MEASUREMENT PLATFORM

A. TRANSMITTER

Fig. 1 shows the configuration of the RF signal transmitter in the experimental platform for IEEE 802.22. In this study, because only the PHY performance was expected to be evaluated, the SCH and FCH—including medium access control (MAC) information—were not used. In other words, the OFDM symbols originally allocated to the SCH and FCH

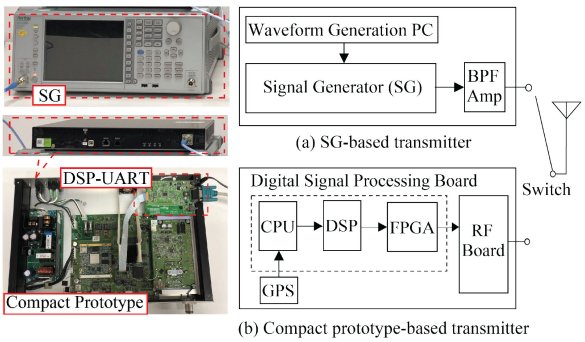

FIGURE 1. Configuration of IEEE 802.22 RF signal transmitter and digital signal generator (upper left: photograph of the SG, upper right: configuration of the SG-based transmitter, middle left: photograph of the compact prototype, lower left: inside photograph of the compact prototype, and lower right: configuration of the compact prototype-based transmitter).

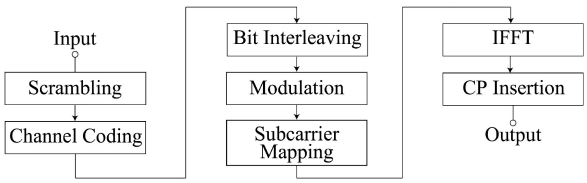

FIGURE 2. Transmitter block diagram of baseband signal in waveform generation PC.

were inserted with the payload data. After generating the baseband signal, the RF board converts the baseband signal to an RF analog signal. An off-the-shelf SG or IEEE 802.22 compact prototype developed in [15] was utilized for the RF signal generation.

To validate the developed receiver, the experimental platform needs to generate a precise transmission signal for the IEEE 802.22 system. As shown in Fig. 1(a), the SG is applied as a signal transmitter because the transmission digital baseband signal used in the computer simulation can be directly emulated and upconverted to the RF analog signal using a SG. The experimental results obtained by using the SG-based transmitter can be used as a reference to validate the analysis using the prototype-based transmitter. The baseband digital signal for the SG can be generated using any data processing software (e.g., MATLAB and LabVIEW) installed on an external waveform generating personal computer (PC) and transferred to the SG through its Ethernet interface. Fig. 2 shows a transmitter block diagram of the baseband signal of the IEEE 802.22 system. The SG can convert the discrete signal into an analog signal using a 14-bit digital-to-analog converter (DAC). Subsequently, the baseband analog signal can be upconverted into an RF analog signal. The generated RF analog signal is transmitted through an SMA-type connector for further processing. Although the SG enables flexible transmission-signal modification, it has some limitations. In general, the external waveform generating PC is necessary to support or arrange baseband signal parameters,

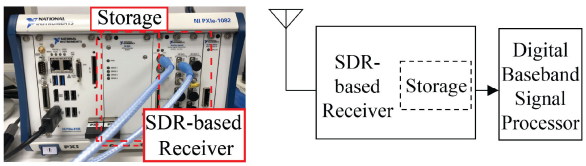

FIGURE 3. Configuration of IEEE 802.22 RF signal receiver and digital signal processor.

and an external power amplifier (Amp) with relatively large power sources is required to amplify the transmission signals, which can be inconvenient, especially during field experiments. Moreover, a band-pass filter (BPF) was not implemented to suppress the out-of-band emission (OOBE) of the transmitted RF analog signal, which could potentially induce interference in the adjacent channel during field experiments. In addition, only a 14-bit DAC was supported in the utilized SG, and a transmitter with a better-resolution DAC would be preferred to reduce undesirable quantum noise.

To cope with the limitations of SGs, a compact IEEE 802.22 prototype was utilized for more realistic PHY evaluation in the laboratory and future field experiments. The IEEE 802.22 prototype developed in [15] could be divided into two parts, that is, the RF and digital signal processing boards, as shown in Fig. 1(b). The PHY parameter was configured, and the baseband signal was generated in the digital signal processing board, comprising a field-programmable gate array (FPGA), digital signal processor (DSP), and central processing unit (CPU). This board generates a standardized IEEE 802.22 PHY signal.

In this study, the same payload data of the repetitions of "0xaa" are used for each frame. Some of the PHY parameters can be simply adapted through an external PC connected to the prototype via the Ethernet interface. For further adaption, an external DSP-based universal asynchronous receiver/transmitter (DSP-UART) board was connected to the prototype and applied to the system parameter configuration. In the RF board, a 16-bit high-resolution DAC was implemented to enhance the dynamic range on the transmitter side [15]. Moreover, the low-pass filter (LPF) and BPF were inserted to reduce the harmonics and OOBE, respectively.

B. SDR-BASED RECEIVER

Fig. 3 shows the configuration of the IEEE 802.22 RF signal receiver in the IEEE 802.22 experimental platform. An SDR device (NI 5644R VST, Vector Signal Transceiver) is used as the RF signal receiver. The SDR device facilitates relatively high flexible signal processing compared with the compact prototype and is suitable for performance evaluation during the receiver algorithm development. The NI VST supports a wide frequency range from 65 MHz to 6 GHz and a bandwidth of up to 80 MHz, sufficient for experimentation with the IEEE 802.22-based system. In addition, four-drive storage is embedded, facilitating post-processing of the received baseband digital signals. After the RF signal is received in the SDR

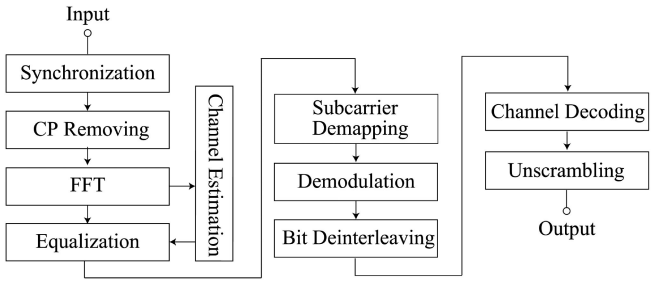

FIGURE 4. Receiver block diagram of baseband signal in digital baseband signal processor of RF signal receiver.

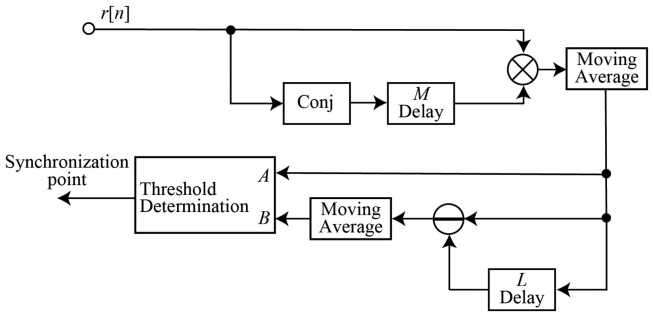

FIGURE 5. Block diagram of the autocorrelation-based synchronization scheme.

device, a BPF is used to eliminate unwanted signals and noise outside of the supported frequency range. The RF signal is then down-converted to a baseband analog signal and sampled into a baseband digital signal using a 16-bit high-resolution analog-to-digital converter. The digital signal is transmitted to the FPGA and embedded four-drive storage for offline post-processing.

C. DIGITAL BASEBAND SIGNAL PROCESSOR

The digital baseband signal processor performs OFDM to recover the transmitted signal using a digitized received baseband signal stored in the SDR-based receiver. Fig. 4 shows a block diagram of the baseband signal receiver in the digital baseband signal processor of the RF signal receiver for the IEEE 802.22 DS signal. First, a timing synchronization algorithm is applied to synchronize the received signal with an STS. In this paper, an autocorrelation-based synchronization scheme and a cross-correlation-based synchronization scheme are provided and analyzed, with reference to [17]. A block diagram of the autocorrelation-based synchronization scheme is shown in Fig. 5. First, the autocorrelation of the received signal is calculated as follows:

$$R_{\mathrm{A}}[n] = r[n]\, r^{*}[n+M], \tag{1}$$

where $r[n]$ is the nth digital sample of the received signal, and M is the length of the STS repetition—that is, $M = 512$ in the IEEE 802.22 system. Then, the moving average of R_{A} with a window length of M can be calculated as follows:

$$R_{\mathrm{M}}[n] = \frac{\sum_{m=1}^{M} |R_{\mathrm{A}}[n+m]|^2}{M}. \tag{2}$$

This step is implemented to generate a mountain-shaped peak over the autocorrelation results, which supports synchronization-point seeking. A sliding differentiator with a step of L can be applied after calculating the moving average as follows:

$$R_{\mathrm{D}}[n] = R_{\mathrm{M}}[n+L] - R_{\mathrm{M}}[n]. \tag{3}$$

Note that $L = 16$ is applied based on [17]. This step is implemented to solve the peak-searching error caused by the plateau of autocorrelation with multiple STSs. Subsequently, a moving average with a window length of $L' = 32$ can be applied to the sliding differentiator as follows:

$$R_{\mathrm{S}}[n] = \frac{\sum_{l=1}^{L'} R_{\mathrm{D}}[n+l]}{L'}. \tag{4}$$

This step is applied to eliminate the effects of the additive white Gaussian noise (AWGN) and Doppler spectrum. Finally, the synchronization point can be determined as the first sample p, which satisfies the following conditions:

$$R_{\mathrm{M}}[p] > A \tag{5}$$

$$R_{\mathrm{S}}[p] < R_{\mathrm{M}}[p] \cdot B \tag{6}$$

where A and B are threshold factors. However, the performance of the autocorrelation synchronization scheme is sensitive to the Doppler spread in a highly mobile communication environment.

Owing to the limitations of the autocorrelation synchronization algorithm, a cross-correlation-based synchronization scheme is proposed. First, the cross-correlation (s_{C}) between the two repetitions of the STS (s_{STS}) and the received digital baseband signal (r) can be calculated as follows:

$$s_{\mathrm{C}}[n] = \sum_{m=0}^{2M-1} s_{\mathrm{STS}}[m]\, r^{*}[m+n] \tag{7}$$

where m and n are the baseband signal sample indices and $(\cdot)^*$ indicates the complex conjugate. Subsequently, the moving average of the cross-correlation can be calculated as follows:

$$s_{\mathrm{A}}[n] = \frac{1}{K} \sum_{k=1}^{K} |s_{\mathrm{C}}[n+k]| \tag{8}$$

where $K = 32$ is the moving-average window size. The synchronization sample index (p) can be determined as the first sample that satisfies the following conditions:

$$|s_{\mathrm{C}}[p]| > \alpha_1 s_{\mathrm{A}}[p+K] \tag{9}$$

$$|s_{\mathrm{C}}[p]| > \alpha_2 |s_{\mathrm{C}}[p-M]| \tag{10}$$

$$\alpha_3 |s_{\mathrm{C}}[p+2M]| > |s_{\mathrm{C}}[p+M]| > \alpha_4 |s_{\mathrm{C}}[p+2M]| \tag{11}$$

where α_1, α_2, α_3, and α_4 are the threshold factors.

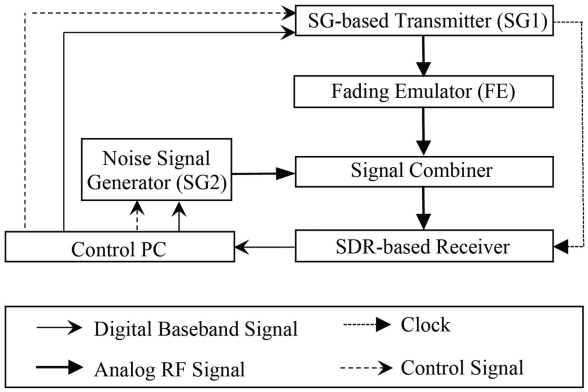

FIGURE 6. Experiment setup of SG-SDR evaluation platform.

In the IEEE 802.22 standard, a carrier frequency accuracy of within ±2 ppm is required at the BS, and the CPE should be synchronized with the BS transmission signal with an accuracy of less than 2% of the subcarrier spacing. After timing synchronization, an autocorrelation algorithm is applied at the CPE to estimate and compensate for the CFO between the BS and CPE [18]. The CFO can be estimated as follows:

$$\hat{f}_{\mathrm{CFO}} = \frac{1}{2\pi M t_{\mathrm{s}}} \arg\left\{ \sum_{q=1}^{Q} \sum_{m=1}^{M} r_{\mathrm{S}}^{*}\left[m+qM\right] r_{\mathrm{S}}\left[m+(q+1)M\right] \right\} \tag{12}$$

where $r_{\mathrm{S}}[n] = r[n+p]$ denotes the synchronized baseband signal. $Q = 4$ is the number of STSs in the superframe preamble, except for the CP, and q is the STS index. In addition, t_{S} is the sampling interval of the baseband signal. After the CFO estimation, the received signal can be compensated for as follows:

$$\hat{r}_{\mathrm{S}}[n] = r_{\mathrm{S}}[n]\, \mathrm{e}^{-\mathrm{j}2\pi \hat{f}_{\mathrm{CFO}} n t_{\mathrm{S}}}. \tag{13}$$

After removing the CP prefixed to each OFDM symbol, the timing- and frequency-synchronized signals are converted from serial data in the time domain to parallel data in the frequency domain by applying an FFT. To compensate for the time-variant multipath fading propagation channel, a pilot-assisted polar linear interpolation and extrapolation-based channel estimation scheme [14] can be applied to reduce the error bits in the extrapolation range and improve the receiver performance. The compensated data are then mapped onto the corresponding subcarrier, and a soft-decision demodulation algorithm is executed in combination with the soft-decision Viterbi algorithm to decode it. Finally, the decoded data are unscrambled.

IV. EXPERIMENTAL SETUP AND EVALUATION RESULTS

A. SG-SDR EVALUATION PLATFORM

The structure of the SG-SDR evaluation platform is shown in Fig. 6, and the devices used for this platform are listed in Table 2. The baseband signal of the IEEE 802.22 DS signal is first generated following the sequence shown in Fig. 2 using MATLAB. Subsequently, the baseband signal is transformed to *.WVI and *.WVD files using the software provided by Anritsu, before being transmitted to the first SG (SG1) via a 1000BASE-T Ethernet cable. The system parameters are listed in Table 3. In regard to the receiver dynamic range, the IEEE 802.22 DS signal was transmitted to the SDR device without additional fading and noise, and the BER performance was measured by adjusting the receive (Rx) power from –95 dBm to –20 dBm. According to the measured dynamic range shown in Fig. 7, a BER of not greater than 10^{-8} was achieved when the Rx power was between –90 and –20 dBm. Therefore, the dynamic range of the SG-SDR platform is estimated to be greater than 70 dB. Generally, a maximum attenuation level of 40 dB in multipath fading and a signal-to-noise radio (SNR) of 30 dB are taken into consideration for the PHY performance evaluation. Hereafter, a transmit (Tx) power of −40 dBm was applied in this study. In parallel, several control signals, including the sampling rate, center frequency, and Tx power, are also transmitted to SG1 through the Ethernet cable. Afterward, SG1 generates the corresponding IEEE 802.22 RF analog signal, and the RF analog signal is input to a multipath FE. The RF analog signal fed through the FE is then combined with the AWGN signal generated by the second SG (SG2). The combined RF signal is then received by the SDR. An external clock—a 10 MHz reference pulse signal generated from SG1—is required for the SDR reduce the CFO and sampling

TABLE 2 Equipment Information

Item	Product model
SG1	Anritsu, MS2830A
SG2	Anritsu, MS2830A
Attenuator (ATT)	Keysight, 8498a
Variable attenuator (VATT)	HP, 8494b
Signal combiner	R&K, PD030-0S
FE	JRC, NJZ-1600D
SDR devices	NI, VST, PXIe-5644r
Base band signal generator and processor	Mathworks, MATLAB (2017b)
Control PC	HP, Probook 450 G3, i7-6500 U CPU, 8G RAM

TABLE 3 System Parameters Applied to Experiment

Item	Value
Communication system	IEEE 802.22 DS
SG1 Tx power	–40 dBm
SG2 Tx power	–40 ~ –70 dBm
ATT	30 dB
VATT	40 dB
Center frequency	473 MHz
Channel bandwidth	6 MHz
Sampling rate	6.856 MHz
Payload modulation	QPSK
CP size	1/4
Velocity	80 km/h (35.6 Hz)

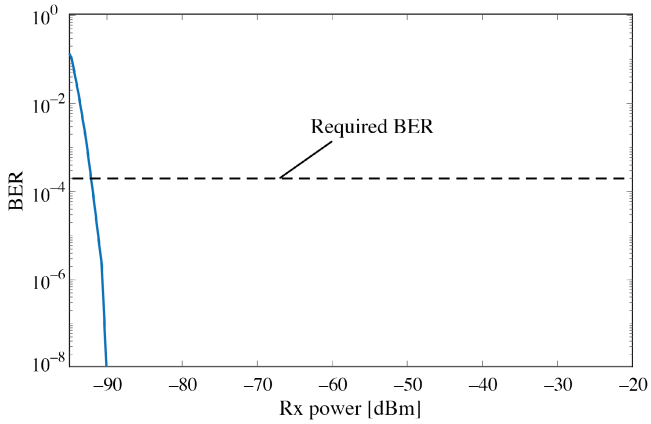

FIGURE 7. Dynamic range of SDR-based receiver.

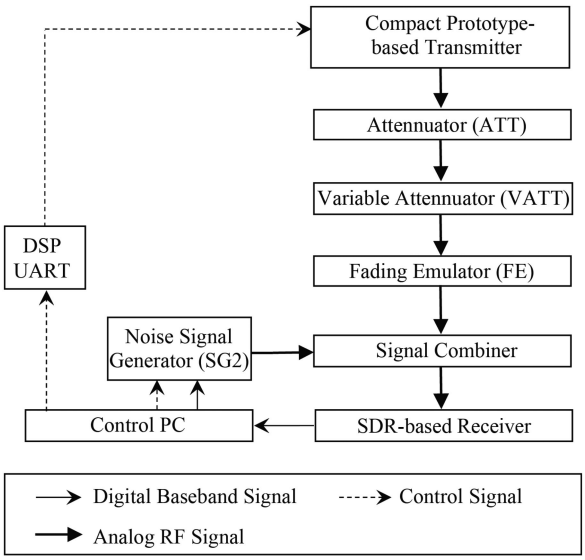

FIGURE 8. Experiment setup of prototype-SDR evaluation platform.

frequency offset. Here, a signal recording program executed by LabVIEW on the embedded control PC in the SDR device must be prepared to record and sample the baseband signal. Because automatic gain control is not supported on the SDR device, an appropriate reference power level must be set on the recording program to avoid signal saturation during dramatic signal fluctuations caused by the relatively high Doppler frequency. Finally, the recorded digital baseband signal is saved in a *.CSV format file and processed using MATLAB on the control PC operating as a DSP.

B. PROTOTYPE SDR EVALUATION PLATFORM

The structure of the prototype SDR evaluation platform is shown in Fig. 8, and the equipment used for this platform are listed in Table 2. The RF signal of the IEEE 802.22 DS signal is generated from the prototype. A DSP-UART is connected to the prototype using a flexible cable and connected to a control PC using a USB cable to modify the system configuration. The configurations of the PHY parameters are listed in Table 3. The corresponding parameters can be modified using TeraTerm (installed on the control PC), sent to the DSP-UART as a control signal, and written to the DSP board of the prototype. The interface between the PHY and upper layers can be shut down by the DSP-UART because only the PHY performance needs to be evaluated in this study. Consequently, header symbols that include MAC information are not considered, and the same data as the payload are embedded by applying the test mode of the prototype, leading to easier analysis at the receiver. In addition, to allow a flexible frame size, the allocation start time of the frame should be changed by modifying the electrically erasable programmable read-only memory (EEPROM) via the DSP-UART. To ensure a safe Rx power level during the measurements, an RF signal of 30 dBm generated from the prototype is first transmitted through a fixed attenuator with a 30 dB attenuation before being attenuated by a variable attenuator with a 40 dB attenuation to obtain the same Tx power as the SG-SDR platform. Subsequently, the attenuated RF signal is transmitted through the FE and is then combined with the AWGN generated by SG2 through a signal combiner. The combined RF signal is received and sampled into digital data using the SDR. Finally, the digital data are processed using MATLAB following the flow shown in Fig. 4.

TABLE 4 WRAN Profile A [19]

Path	1	2	3	4	5	6
Delay (μs)	0	3	8	11	13	21
Relative amplitude (dB)	0	–7	–15	–22	–24	–19

C. PROPAGATION CHANNEL

In this study, an FE (NJZ-1600D) was used to simulate the propagation channel. The NJZ-1600D can simulate the fading channel for an RF band signal with a bandwidth of up to 20 MHz. A delay profile with up to 12 paths is supported, and both Rayleigh distribution-based fading and Rice distribution-based fading are supported and can be individually set for each path. In this study, a delay profile of the WRAN Profile A with six paths [19] was applied as the multipath channel to imitate the propagation environment in rural areas. The parameters of the WRAN Profile A are listed in Table 4. Rayleigh distribution-based fading was applied for each path.

D. FRAME STRUCTURE CONFIGURATION

To separately analyze the performance of the receiving schemes of the proposed highly mobile IEEE 802.22 communication system—that is, the timing synchronization, frequency synchronization, and channel estimation schemes—several frame structure configuration modes were applied.

1) MODE 1

To analyze the performance of the time-synchronization schemes—for example, the time-synchronization error—, an

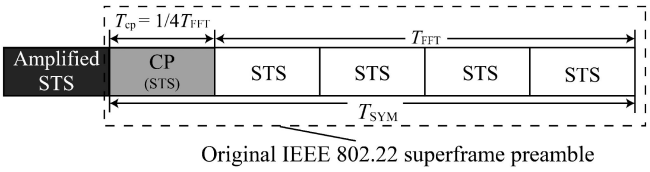

FIGURE 9. Modified superframe preamble of frame structure configuration Mode 1.

TABLE 5 Number of OFDM Symbols in Each DS Subframes

Case	Number of OFDM symbols in each DS subframe
1	9
2	11
3	13
4	15
5	17

ideal synchronization point in the received digital baseband data is required. However, it can be difficult to obtain ideal synchronization points in experimental measurements. To solve this problem, a modified prefix for the superframe preamble was applied, as shown in Fig. 9. In Mode 1, an extra repetition of the STS amplified by 3 dB is prefixed to the superframe preamble, and a cross-correlation algorithm is conducted to assist the synchronization-point searching. The cross-correlation (s'_c) between an STS (s_{STS}) and the received digital baseband signal (r) can be calculated as follows:

$$s'_c[n] = \sum_{m=0}^{M-1} s_{STS}[m]\, r^*[m+n]. \tag{14}$$

Because the measured channel is always active, the peak of s'_c within a superframe can be determined as the pseudo-ideal synchronization point with an amplified STS. After determining the pseudo-ideal synchronization point, the prefixed amplified STSs are removed. The rest of the signal is processed using the digital baseband signal processor described in subsection III.C.

2) MODE 2

To evaluate the system performance based on IEEE 802.22, the frame configuration complied with the frame structure described in Section II.

With a 6 MHz bandwidth and a 1/4 CP length, the number of OFDM symbols per frame was 26 in each frame. Based on the standard, the number of OFDM symbols allocated to the US subframe must be greater than seven. The number of OFDM symbols in each DS subframe supports various asymmetric throughput requirements between the DS and the US. In this study, to validate the robustness and feasibility of the receiver with a flexible DS subframe size, several subframe allocation schemes were applied, as listed in Table 5.

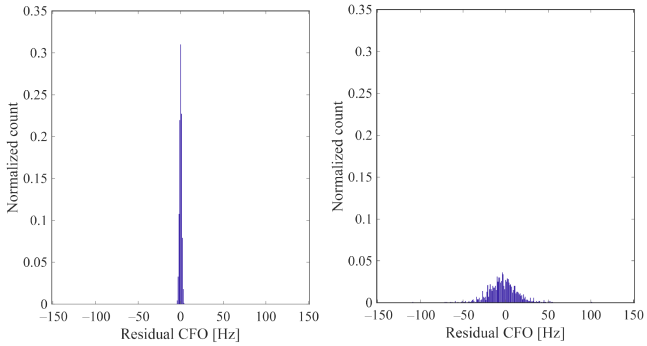

(a) AWGN channel (b) WRAN Profile A channel

FIGURE 10. Residual CFO by applying the frequency synchronization scheme. (a) AWGN channel. (b) WRAN Profile A channel.

E. EVALUATION RESULTS

First, the performance of the frequency synchronization scheme was evaluated by applying the frame structure configuration Mode 1 and DS subframe size Case 4 with the SG-SDR platform. Pseudo-ideal timing synchronization was applied. The system parameters used for the measurements are listed in Table 3. In addition, a CFO of 1892 Hz was manually added to the system by configuring a +2 and –2 ppm frequency offset at the SG and SDR devices, respectively. Fig. 10(a) and (b) show histogram plots of the residual CFO after applying the frequency synchronization scheme with an SNR of 30 dB at rest (0 km/h) and in a multipath fading environment at a velocity of 80 km/h. Here, the bin width of the histogram is 1 Hz. As shown in Fig. 10(a), the residual CFO is trivial within ±7 Hz in the AWGN channel (without multipath fading). Meanwhile, the high velocity and multipath fading degrade the accuracy of the estimated CFO, the residual CFO occasionally exceeding ±67 Hz, as shown in Fig. 10(b). The standard deviation of the residual CFO is approximately 17.8 Hz, and more than 99.7% of the snapshots are within ±67 Hz based on the 3-sigma rule that meets the requirement of 2% of the subcarrier spacing.

The performance of the channel estimation scheme can then be evaluated by applying the Mode 1 frame structure configuration with the flexible DS subframe size as listed in Table 5. The measurement can be performed using the PHY parameters listed in Table 3 with the SG-SDR and prototype SDR experimental platforms, as shown in Figs. 6 and 8, respectively. Here, a pseudo-ideal timing synchronization has been applied. Fig. 11 shows the BER performance in a long-delay multipath fading environment, assuming a relatively high velocity of 80 km/h. The measurement results with the developed SG-SDR platform exhibited are similar to the computer simulations. Compared with the measurement results of the SG-SDR platform, the results of the prototype SDR platform were slightly degraded by approximately 1 dB owing to the CFO. Moreover, the difference in the BER characteristics between various frame sizes was also within 1 dB. With an SNR of approximately 21 dB, the required BER

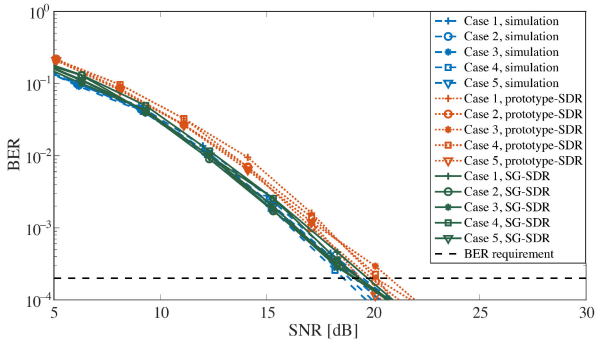

FIGURE 11. SNR vs. BER characteristics by computer simulation and the proposed evaluation platform with frame structure configuration Mode 1.

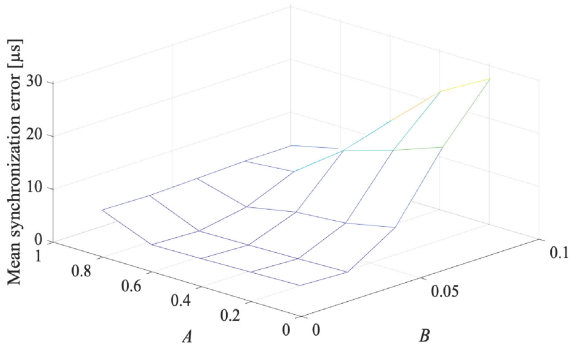

FIGURE 12. Mean synchronization error with various threshold factor values.

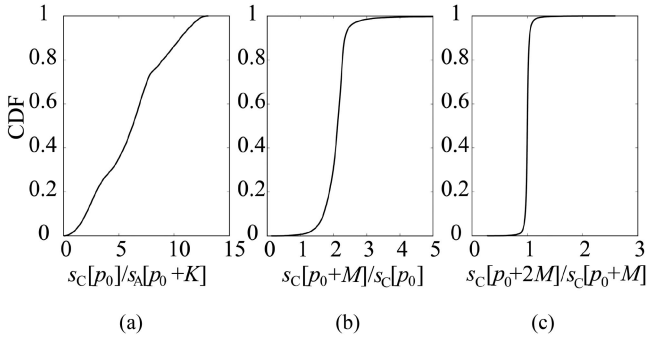

FIGURE 13. CDF of $\frac{s_C[p_0]}{s_A[p_0+K]}$, $\frac{s_C[p_0+M]}{s_C[p_0]}$, and $\frac{s_C[p_0+2M]}{s_C[p_0+M]}$ when SNR = 24 dB.

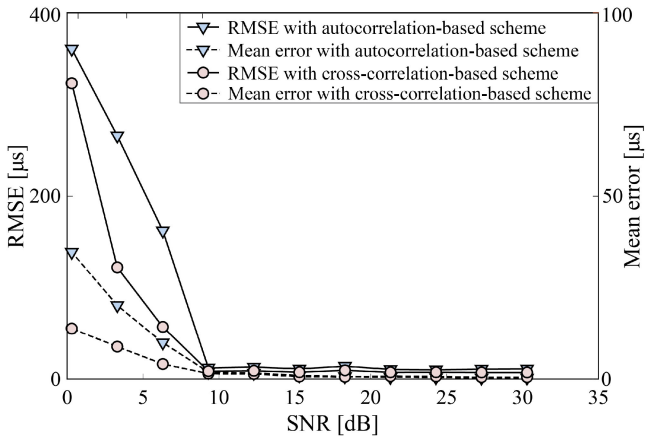

FIGURE 14. Synchronization error of the autocorrelation- and cross-correlation-based timing synchronization scheme.

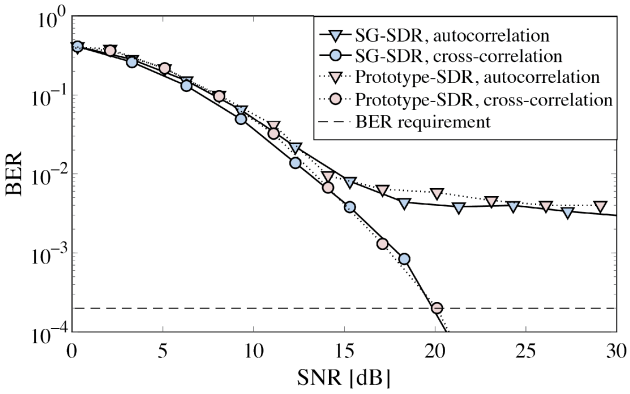

FIGURE 15. SNR vs. BER characteristics by the proposed evaluation platform with frame structure configuration Mode 2.

of 2×10^{-4} was achieved, demonstrating the robustness of the channel estimation scheme.

Thereafter, the proposed time-synchronization schemes were evaluated by applying the Mode 1 frame structure configuration with the DS subframe size Case 4 using the SG-SDR experimental platform shown in Fig. 6. The system parameters used for the measurements are listed in Table 3. The mean synchronization error with various values, as shown in Fig. 12, can be used to determine the threshold factors A and B of the autocorrelation-based time-synchronization scheme. As a result, $A = 0.7$ and $B = 0.03$, were used.

To determine the threshold factors α_1, α_2, α_3, and α_4 of the cross-correlation-based time synchronization scheme, the cumulative distribution functions (CDFs) of $\frac{s_C[p_0]}{s_A[p_0+K]}$, $\frac{s_C[p_0+M]}{s_C[p_0]}$, and $\frac{s_C[p_0+2M]}{s_C[p_0+M]}$ with an SNR of 24 dB are shown in Fig. 13(a)–(c), respectively, where p_0 is the pseudo-ideal synchronization point after removing the prefixed amplified STSs. As the result, $\alpha_1 = 5$, $\alpha_2 = 1.5$, $\alpha_3 = 1.2$, and $\alpha_4 = 0.8$ were used.

The root mean square error (RMSE) and mean error of the frame synchronization with the proposed autocorrelation-based and cross-correlation-based timing synchronization schemes are shown in Fig. 14. The RMSE of the synchronization error decreases with the increase in the SNR. In addition, the cross-correlation-based scheme achieves better performance than the autocorrelation-based scheme using the SG-SDR experimental platform.

Ultimately, the performance of the digital baseband signal processor was comprehensively evaluated by applying the Mode 2 frame structure configuration and DS subframe size Case 4. Fig. 15 shows the BER characteristics of both the SG-SDR and prototype SDR experimental platforms, The difference between the two platforms is within 1 dB of the

cross-correlation-based timing synchronization scheme, similar to the results obtained with perfect timing synchronization. With the autocorrelation-based synchronization scheme, the required BER of 2×10^{-4} could not be achieved even at a high SNR of 30 dB. Using the cross-correlation-based synchronization scheme, the required BER could be achieved when the SNR was approximately 20 dB. Thus, we demonstrated the feasibility of the proposed experimental platform and digital baseband signal processor for a highly mobile IEEE 802.22 system.

V. CONCLUSION

In this study, an SDR-based platform was developed to evaluate the PHY performance of a highly mobile IEEE 802.22 communication system. The framework of the baseband SG and processor was implemented completely using software and programmable hardware, enabling simple utilization, algorithm modification, and debugging. To enable the platform, we established a LabVIEW-based program to record and store the baseband signal received by the SDR device, and a MATLAB-based program for offline post-processing of the recorded IEEE 802.22 baseband signal. As a result, the proposed prototype SDR platform exhibited performance was similar to that of computer simulations and the SG-SDR platform. Consequently, the proposed platform can be expected to be used for PHY performance evaluation in the development of receiver algorithms and future field experiments. Based on the laboratory experiment results, by applying the developed SDR-based receiver and the proposed receiving schemes, the transmitted signal IEEE 802.22 DS from the SG was successfully received with a required BER of 2×10^{-4} at a high velocity of 80 km/h in a long-delay 6-path propagation environment. Consequently, the feasibility of highly mobile IEEE 802.22 communication was demonstrated. Moreover, our proposed platform is expected to be implemented in the field experiment as future works.

REFERENCES

[1] R. Ouyang, T. Matsumura, K. Mizutani, and H. Harada, "Development of evaluation platform for IEEE 802.22-based highly mobile WRAN communication system with an SDR-based receiver," in *Proc. 23rd Int. Symp. Wireless Pers. Multimedia Commun.*, Oct. 2020, pp. 1–6.

[2] K. Abboud, H. Omar, and W. Zhuang, "Interworking of DSRC and cellular network technologies for V2X communications: A survey," *IEEE Trans Veh. Technol.*, vol. 65, no. 12, pp. 9457–9470, Dec. 2016.

[3] *IEEE Standard for Information Technology – Telecommunications and Information Exchange Between Systems Local And Metropolitan Area Networks Specific Requirements Part 11: Wireless LAN Medium Access Control (MAC) and Physical Layer (PHY) Specifications Amendment 6: Wireless Access in Vehicular Environments Sponsor: LAN/MAN Standards Committee of the IEEE Computer Society*, Jun. 2010.

[4] ARIB, "700 MHz band intelligent transport systems," ARIB, STD T109-v1.2, Dec. 2013.

[5] 3GPP, "Study on LTE-based V2X services (v14.0.0, release 14)," Tech. Rep. 36.885, Jul. 2016.

[6] 3GPP, "Study on NR vehicle-to-everything (V2X) (v16.0.0, release 16)," Mar. 2019.

[7] R. Atallah, M. Khabbaz, and C. Assi, "Multihop V2I communications: A feasibility study, modeling, and performance analysis," *IEEE Trans. Veh. Technol.*, vol. 66, no. 3, pp. 2801–2810, Mar. 2016.

[8] W. Anwar, N. Franchi, and G. Fettweis, "Physical layer evaluation of V2X communications technologies: 5G NR-V2X, LTE-V2X, IEEE 802.11bd, and IEEE 802.11p," in *Proc. IEEE 90th Veh. Technol. Conf. (VTC2019-Fall)*, 2019, pp. 1–7.

[9] H. Harada, "White space communication systems: An overview of regulation, standardization and trial," *IEICE Trans. Commun.*, vol. 97, no. 2, pp. 261–274, Feb. 2014.

[10] A. Ali, W. Hamouda, and M. Uysal, "Next generation M2M cellular networks: Challenges and practical considerations," *IEEE Commun. Mag.*, vol. 53, no. 9, pp. 18–24, Sep. 2015.

[11] Y. Han, E. Ekici, H. Kremo, and O. Altintas, "Resource allocation algorithms supporting coexistence of cognitive vehicular and IEEE 802.22 networks," *IEEE Trans. Wireless Commun.*, vol. 16, no. 2, pp. 1066–1079, Feb. 2017.

[12] *IEEE Standard for Information Technology–Telecommunications and Information Exchange Between Systems Wireless Regional Area Networks (WRAN) Specific Requirements—Part 22: Cognitive Wireless RAN Medium Access Control (MAC) and Physical Layer (PHY) Specifications: Policies and Procedures for Operation in the TV bands*, Jul. 2011.

[13] R. Ouyang, T. Matsumura, K. Mizutani, and H. Harada, "A robust channel estimation for IEEE 802.22 enabling wide area vehicular communication," in *Proc. 21st Int. Symp. Wireless Pers. Multimedia Commun.*, Nov. 2018, pp. 52–57.

[14] R. Ouyang, T. Matsumura, K. Mizutani, and H. Harada, "A reliable channel estimation scheme using scattered pilot pattern for IEEE 802.22-based mobile communication system," *IEEE Trans. Cogn. Commun. Netw.*, vol. 5, no. 4, pp. 935–948, Dec. 2019.

[15] T. Matsumura, H. Ueno, K. Mizutani, and H. Harada, "Compact IEEE 802.22-based radio equipment enabling easy installation for regional area network system using TV white-spaces," in *Proc. IEEE Int. Symp. Local Metrop. Area Netw.*, Jun. 2017, pp. 1–6.

[16] A. Bishnu and V. Bhatia, "An IEEE 802.22 transceiver framework and its performance analysis on software defined radio for TV white space," *Telecommun. Syst.*, vol. 68, no. 4, pp. 657–668, Aug. 2018.

[17] D. Wang and J. Zhang, "Timing synchronization for MIMO-OFDM WLAN systems," in *Proc. IEEE Wireless Commun. Netw. Conf.*, Jun. 2007, pp. 1177–1182.

[18] T. Kim and S. Park, "A new symbol timing and frequency synchronization design for OFDM-based WLAN systems," in *Proc. 9th Int. Conf. Adv. Commun. Technol.*, Feb. 2007, pp. 1669–1672.

[19] E. Sofer and G. Chouinard, *WRAN Channel Modeling*, IEEE 802.22-05/0055r7, Aug. 2005.

RUITING OUYANG (Member, IEEE) received the B.E. degree in communication science and engineering from Fudan University, Shanghai, China, and the M.I. and Ph.D. degrees in communications and computer engineering from Kyoto University, Kyoto, Japan, in 2018 and 2021, respectively. She currently a Researcher with Kyoto University. She is currently researches on the topic of the development of IEEE 802.22-based mobile communication system.

TAKESHI MATSUMURA (Member, IEEE) received the M.E. degree in electronic engineering and the Ph.D. degree in nano-mechanics engineering from Tohoku University, Sendai, Japan, in 1998 and 2010, respectively. From 1998 to 2007, he was engaged in the research and development of wireless communications devices in some companies. In 2007, he joined the National Institute of Information and Communications Technology, as a Researcher with Smart Wireless Laboratory and engaged in the white-space communication systems and 5th generation mobile communication systems. During 2016–2019, he was an Associate Professor with the Graduate School of Informatics, Kyoto University, Kyoto, Japan. He is currently the Director with Wireless Systems Laboratory, Wireless Networks Research Center, Network Research Institute, NICT. He is also a Researcher with Kyoto University. His research interests include white-space communication systems, wide-area wireless network systems, and beyond 5G mobile communication systems, and wireless emulation technologies. He was the recipient of the Best Paper Award from IEEE LANMAN 2017.

KEIICHI MIZUTANI (Member, IEEE) received the B.E. degree in electric, electrical and system engineering from Osaka Prefecture University, Sakai, Japan, in 2007, and the M.E. and Ph.D. degrees in electric and electrical engineering from the Tokyo Institute of Technology, Tokyo, Japan, in 2009 and 2012, respectively. He is currently an Associate Professor with Kyoto University, Kyoto, Japan. In 2010, he was an Invited Researcher with Fraunhofer Heinrich Hertz Institute, Germany. From April 2012 to September 2014, he was a Researcher with the National Institute of Information and Communications Technology (NICT). He is currently researches on the topics of physical layer technologies in white space communications, dynamic spectrum access, wireless smart utility networks (Wi-SUN), and 4G/5G/beyond 5G systems including OFDM, OFDMA, MIMO, and multi-hop relay network systems. Since joining in NICT, he has been involved in IEEE 802 standardization activities, namely 802.11af, 802.15.4m, and 802.22b. He was the recipient of the Special Technical Awards from IEICE SR Technical Committee in 2009 and 2017, Best Paper Award from IEICE SR Technical Committee in 2010, Young Researcher's Award from IEICE SRW Technical Committee in 2016, and Best Paper Award from WPMC2017.

HIROSHI HARADA (Member, IEEE) is currently a Professor with the Graduate School of Informatics, Kyoto University, Kyoto, Japan, and an Executive Research Director of the Social ICT Research Center, National Institute of Information and Communications Technology (NICT). In 1995, he joined the Communications Research Laboratory, Ministry of Posts and Communications (currently, NICT). From 2005 to 2014, he was a Visiting Professor with the University of Electro-Communications, Tokyo, Japan. He has authored the book entitled *Simulation and Software Radio for Mobile Communications* (Artech House, 2002). Since 1995, he has been researching on software defined radio, cognitive radio, dynamic spectrum access network, wireless smart ubiquitous network, and broadband wireless access systems on the microwave and millimeter-wave band. He also has joined many standardization committees and forums in the United States and also in Japan and fulfilled important roles for them, especially IEEE 1900 and IEEE 802. He was the Chair of IEEE DySpan Standards Committee and the Vice Chair of IEEE 802.15.4g, IEEE 802.15.4m, 1900.4, and TIA TR-51. He was a Board of Directors of IEEE Communication Society Standards Board, SDR forum, DSA alliance, and WhiteSpace alliance. He is a Co-Founder of Wi-SUN alliance and was the chairman of the board from 2012 to 2019. He is currently the Vice Chair of IEEE 2857, IEEE 802.15.4aa, and Wi-SUN alliance. He was the Chair of IEICE Technical Committee on Software Radio (TCSR) and the Chair of Public Broadband Mobile Communication Development Committee, ARIB. He is also involved in many other activities related to telecommunications. He was the recipient of the achievement awards in 2006 and 2018 and a Fellow of IEICE in 2009, respectively, and the achievement awards of ARIB in 2009 and 2018, respectively, on the topic of research and development on cognitive radio and wireless smart utility network.